



Durham E-Theses

N-body realizations of cuspy dark matter haloes

Kazantzidis, Stelios

How to cite:

Kazantzidis, Stelios (2002) *N-body realizations of cuspy dark matter haloes*, Durham theses, Durham University. Available at Durham E-Theses Online: <http://etheses.dur.ac.uk/4141/>

Use policy

The full-text may be used and/or reproduced, and given to third parties in any format or medium, without prior permission or charge, for personal research or study, educational, or not-for-profit purposes provided that:

- a full bibliographic reference is made to the original source
- a [link](#) is made to the metadata record in Durham E-Theses
- the full-text is not changed in any way

The full-text must not be sold in any format or medium without the formal permission of the copyright holders.

Please consult the [full Durham E-Theses policy](#) for further details.

N-body Realizations of Cuspy Dark Matter Haloes

Stelios Kazantzidis

A thesis submitted to the University of Durham
in accordance with the regulations for admission to the
Degree of Master of Science by Research and Thesis.

The copyright of this thesis rests with the author.
No quotation from it should be published without his prior
written consent, and information derived from it should
be acknowledged.

The copyright of this thesis rests with the author.
No quotation from it should be published without
his prior written consent and information derived
from it should be acknowledged.



24 MAR 2003

University of Durham
2002

Abstract: N-body Realizations of Cuspy Dark Matter Haloes

by Stelios Kazantzidis

We describe an algorithm for generating equilibrium initial conditions for numerical experiments with dark matter haloes. Our haloes are modelled using a general form for the mass density $\rho(r)$, making it possible to represent most of the popular density profiles in the literature. The finite mass γ -models and the cuspy density profiles found in recent high-resolution cosmological N -body simulations having a density power-law fall-off at large distances proportional to r^{-3} are included as special cases. The algorithm calculates the phase-space distribution function of each model assuming spherical symmetry and either an isotropic velocity dispersion tensor or an anisotropic velocity dispersion tensor of the type proposed by Osipkov and Merritt. The particle velocities are assigned according to the exact velocity distribution, making this method ideal for experiments requiring a high degree of stability. Numerical tests confirm that the resulting models are highly stable. This approach is motivated by the instabilities that arise when a local Maxwellian velocity distribution is adopted. For example, after approximating the velocity distribution by a Gaussian we show that a Hernquist halo with an initial r^{-1} density cusp immediately develops a constant density core. Moreover, after a single crossing time the orbital anisotropy has evolved over the entire system. Previous studies that use this approximation to construct halo or galaxy models could be compromised by this behaviour.

Using the derived distribution functions we show the exact 1-d velocity distributions and we compare them with the Gaussian velocity distributions with the same second moment for different distances from the halo centre. We show that instabilities arise because a Gaussian velocity distribution is a very poor approximation to the true velocity distribution of particles. We also perform a series of numerical simulations evolving several dark matter halo models in isolation, with the intention of checking the stability of the initialization procedure in both configuration and velocity space. A subset of the models are evolved under the assumption that

the velocity distribution at any given point is a Gaussian and the time evolution of the density profiles and velocity structure is monitored. Finally, a number of applications are discussed, including issues of relaxation in dark matter haloes as well as mergers of haloes in scattering experiments.

Contents

Abstract	i
1 Introduction	1
2 Initialization Procedure	5
2.1 Introduction	5
2.2 Density Profiles	5
2.3 Model Truncation	7
2.4 Distribution Function Calculation	8
2.4.1 Isotropic Models	9
2.4.2 Anisotropic Models of the Osipkov-Merritt Type	10
2.5 Generation of Initial Conditions	11
3 N-body Realizations of Halo Models	13
3.1 Preliminaries	13
3.2 Models Generated Under the Local Maxwellian Approximation	14
3.3 Velocity Profiles	16
3.4 Stability Tests Using the Exact Distribution Function	22
4 Applications	27
4.1 Collisions of DM Haloes	27
4.2 Relaxation and Evolution of Substructure in Cuspy DM Haloes	28
4.3 Stability Studies	29
4.4 Multicomponent Models	29
5 Conclusions	31
6 Computer Programs Available	33
7 The Moore Density Profile	34

List of Figures

3.1	Evolution of density profile and velocity structure for model A	16
3.2	Evolution of velocity structure for an isotropic and an anisotropic Hernquist profile	17
3.3	One dimensional velocity distribution for an isotropic Hernquist profile .	18
3.4	One dimensional velocity distribution for an isotropic NFW profile . . .	19
3.5	One dimensional velocity distribution for an isotropic Moore profile . . .	20
3.6	Ratios between the true velocity distributions and the Gaussians for an NFW and a Moore profile	21
3.7	Evolution of density profile and velocity structure for model B	22
3.8	Evolution of density profile and velocity structure for model C	23
3.9	Evolution of density profile and velocity structure for model D	24
3.10	Evolution of density profile and velocity structure for model E	26

Acknowledgements

It is a great pleasure to thank my thesis advisors Professor Ben Moore from the Institute for Theoretical Physics at the University of Zürich and Dr. John Magorrian from the Department of Physics at the University of Durham for the suggestion of the topic of my thesis. I especially want to thank Professor Ben Moore for offering me a research position and for his valuable support, advice, and help I enjoyed over the period of this work. I am particularly indebted to Dr. John Magorrian foremostly for his vigilant supervision and help with the technical details. Our innumerable discussions allowed me to develop my understanding of the details of this work.

I am very grateful to all the members of the Extragalactic Astronomy and Cosmology group of the Department of Physics at the University of Durham and most notably to Professor Carlos Frenk for allowing me to work and interact with his group. I consider privileged anyone who had the opportunity to interact with scientists of such excellence. I take the opportunity to express my gratitude to Dr. Vincent Eke, distinguished member of the aforementioned group, who has had a great influence on how I think about research in Astrophysics. Our fruitful discussions and his tremendous help are deeply appreciated. In addition, I would like to recognize the continuous support of Dr. Lydia Heck, computer officer at the Institute for Computational Cosmology (ICC).

Further, I would like to acknowledge the kind hospitality of the Institute for Theoretical Physics at the University of Zürich during my visits there. I am grateful to the members of the Institute and the director Professor Daniel Wyler for welcoming me wholeheartedly.

Finally, I wish to express my deepest gratitude to my parents and my wife for their unconditional support and encouragement. Without them the completion of this work would have been far more arduous.

Preface

*N-body Realizations of Cuspy Dark Matter Halo*s

The work described in this thesis was undertaken between October 2001 and September 2002 whilst the author was a research student under the supervision of Professor Ben Moore and Dr. John Magorrian in the Department of Physics at the University of Durham. This work has not been submitted for any other degree at this (or any other) university.

The software that has been developed in the course of this study is the author's own work. Collaborators involved in this thesis are Professor B. Moore & Dr. S.J. Magorrian.

Results from chapter 3 will be submitted in ApJ :

- Kazantzidis, S., Magorrian, S.J., & Moore, B., 2002, in preparation

Chapter 1

Introduction

The fundamental equation that governs the evolution of a collisionless stellar system is the Collisionless Boltzmann Equation (hereafter, CBE) (also known as the Vlasov Equation),

$$\frac{df}{dt} \equiv \frac{\partial f}{\partial t} + \mathbf{v} \cdot \nabla f - \nabla \Phi \cdot \frac{\partial f}{\partial \mathbf{v}} = 0. \quad (1.1)$$

where $\Phi(r)$ is the smooth overall gravitational potential and $f(\mathbf{r}, \mathbf{v}, t)$ is the phase-space distribution function (hereafter, DF), defined such that $f(\mathbf{r}, \mathbf{v}, t) \Delta^3 \mathbf{r} \Delta^3 \mathbf{v}$ is the expectation value of the mass of the stellar system within a small volume $\Delta^3 \mathbf{r} \Delta^3 \mathbf{v}$ of the phase space at time t .

The importance of the DF in the dynamical study of collisionless stellar systems follows directly from inspecting equation (1.1): for a stellar system in equilibrium the DF constitutes a steady-state solution of the CBE. Essential to the task of making an educated guess as to the functional form of the DF is the Jeans' theorem stating that any equilibrium solution of the CBE and thus the DF itself depends on the phase space coordinates (\mathbf{r}, \mathbf{v}) only through the integrals of motion. For a spherically symmetric stellar system in equilibrium, these integrals are given by the energy per unit mass, E , and the absolute value of the angular momentum vector per unit mass, L ; $f = f(E, L)$ (Lynden-Bell 1962; Binney & Tremaine 1987; hereafter BT). The mass density of the stellar system is then given by,

$$\rho(r) = \iiint f(E, L) d^3 \mathbf{v}. \quad (1.2)$$

Equation (1.2) is known as the fundamental integral equation and its inversion generates the DF for a given density profile $\rho(r)$. The mass density of equation (1.2) depends implicitly on the system's gravitational potential, $\Phi(r)$, and these two quantities are related through Poisson's equation,

$$\nabla^2 \Phi(r) = 4\pi G \rho(r). \quad (1.3)$$



Models for stellar systems based on the solution of the equations (1.2) and (1.3) are called self-consistent models.

There are two general approaches to generating self-consistent equilibria. In the first, known as "*f* to ρ approach", one assumes a plausible form for the DF, and then solves equations (1.2) and (1.3) simultaneously, subject to reasonable boundary conditions on Φ . Examples of this approach are the spherical models of King (1966) and the axisymmetric models of Kuijken & Dubinski (1994). The drawback of this approach is that one typically has only limited control over the resulting density profile. Alternatively, in the " ρ to *f* approach", one takes the desired $\rho(r)$ and $\Phi(r)$ along with a very general assumption about the form of the DF (e.g., that it has no L dependence) and then inverts equation (1.2) deriving the DF that self-consistently generates the density profile. This is the approach we adopt in this thesis. Having the DF, it is in principle straightforward to initialize particle positions and velocities in order to generate an N -body realization of a halo.

Despite the inexorable increase in the dynamic range of current cosmological N -body simulations, there are many applications in which one would like to have a more detailed understanding of how isolated haloes evolve and respond to their environment. Examples include the study of relaxation within dark matter (hereafter, DM) haloes (Moore, Katz & Lake 1996a; Hayashi et al. 2002), the orbital decay of satellites (van den Bosch et al. 1999; Colpi, Mayer & Governato 1999), the tidal stripping of mass from DM haloes (Velázquez & White 1995; Mayer et al. 2002), the stability of disks to bar instabilities (Mihos, McGaugh & de Blok 1997), the heating of galactic disks by sinking satellites or DM substructures (Quinn & Goodman 1985; Velázquez & White 1999; Taylor & Babul 2001; Font et al. 2001), encounters and mergers between DM haloes (Aguilar & White 1985; Funato & Makino 1999). In the great majority of these studies a simple way of generating N -body realizations of models has been exploited. This technique involves the computation of some of the velocity moments and the approximation of the DF in velocity space by forms having these moments. In particular, the Jeans equations are solved for each component of the model and the velocity dispersions $\sigma_r(r)$, $\sigma_\theta(r)$, and $\sigma_\phi(r)$ are computed at any given point in space. Assuming that the DF is locally Maxwellian with these

velocity dispersions, the particle velocities are trivially initialized by drawing from Gaussians with these dispersions (see, e.g., Hernquist 1993 for a clear description of this scheme). The advantage of this approximate scheme is that it is relatively easy to implement and generalize (see, e.g., Boily, Kroupa & Peñarrubia 2001 for a generalization to include axisymmetric bulges and haloes) but it suffers from the fact that the resulting model is not in equilibrium – the proper self-consistent velocity profile can often be strongly non-Gaussian, especially near the centre. As we will show, when such a model is evolved using an N -body code, the velocity and density distributions of particles evolve rapidly away from the initial state.

Many studies require a high degree of stability at the halo centre. For example, disks are dynamically cold systems that are susceptible to instabilities and therefore it is important to have a high degree of stability within the inner few percent of the mass distribution. The study of satellite disruption depends sensitively on the density profile of the DM halo (Moore et al. 1996a). Cuspy mass distributions are hard to disrupt, whereas haloes with constant density cores were responsible for the overmerging problem, that is the apparent absence of substructure in the virialized objects reflecting the fact that simulated galaxies seem to merge much more efficiently than real galaxies in groups and clusters (Moore et al. 1996a). Studies of satellite disruption within DM haloes may therefore be compromised by numerical effects. After these considerations, we have been motivated to develop a more accurate method for generating equilibrium N -body systems with arbitrary density profiles. We wanted to disentangle the generation of IC's from the existence of analytical DF's, simple potential-density pairs, and isotropic velocity distributions and thus enable ourselves to produce a more accurate representation of DM halo models.

This thesis is organized as follows. In Chapter 2, we introduce a general parametrization of the halo density profile. We describe how to find both isotropic and anisotropic DF's that self-consistently fit these density profiles and how to generate N -body realizations of these models. Chapter 3 contains N -body realizations of various model haloes and tests of equilibrium. We discuss several possible applications of our models in Chapter 4, before concluding in Chapter 5. In the Appendix, using standard dynamical theory we derive some basic properties of spherical sys-

tems whose density profile follows the Moore et al. (1999, hereafter M99) density profile.

Chapter 2

Initialization Procedure

2.1 Introduction

In order to construct N -body realizations of DM haloes, we must initialize both the velocities and the positions of the particles, thus fully determining the initial conditions (hereafter, IC's) of our models. In principle, the procedure described here can be applied to any density profile whose DF satisfies the minimum requirement for a stellar model to be physical, that is to be everywhere non-negative.

2.2 Density Profiles

According to the standard paradigm of hierarchical structure formation, structures in the Universe form via merging and accretion of smaller systems (White & Rees 1978). According to this scenario, galaxies form in the central regions of DM haloes. Analytical derivations of halo density profiles are extremely difficult because one needs to work in the non-linear regime of the growth of gravitational instabilities. Since the analytical treatment is intricate, many authors have resorted to numerical simulations in order to properly study the structure of DM haloes. These studies (Dubinski & Carlberg 1991; Navarro, Frenk, & White 1996 (hereafter, NFW); Fukushige & Makino 1997; Moore et al. 1998; M99) led to cuspy density profiles that can be fitted by the general formula (Zhao 1996; Kravtsov et al. 1998),

$$\frac{\rho(r)}{\rho_c^0} = \frac{\delta_{\text{char}}}{(r/r_s)^\gamma [1 + (r/r_s)^\alpha]^{(\beta-\gamma)/\alpha}} \quad (r \leq r_{\text{vir}}), \quad (2.1)$$

where ρ_c^0 is the present value of the critical density for closure. This general density profile has a single fitting parameter, the characteristic density δ_{char} . Here, γ , controls the central slope of the profile, β the outer slope, and α characterizes the transition between the inner and outer profile with larger values of α corresponding

to a sharper transition. The logarithmic slope of this profile is given by,

$$\frac{d \ln \rho}{d \ln r} = -\gamma - (\beta - \gamma) \frac{(r/r_s)^\alpha}{[1 + (r/r_s)^\alpha]} . \quad (2.2)$$

An important parameter that is used to characterize the DM haloes is the concentration c , which depends on the mass of the DM halo and the initial power spectrum of density fluctuations. For initial power spectra corresponding to hierarchical formation models the trend is that objects with higher mass have a lower value of concentration. The scale radius of the density profile, r_s , is defined by,

$$r_s = \frac{r_{\text{vir}}}{c} , \quad (2.3)$$

where r_{vir} is the virial radius and is defined as the distance from the centre of the halo within which the mean enclosed density is Δ times the critical one at the epoch at which the halo is viewed. However, since in this work we mainly study the halos at the present epoch, it is equivalent to the present critical density, ρ_c^0 . Quite often, the virial radius is taken to be r_{200} , namely the radius with mean enclosed density $200\rho_c^0$. The scale radius corresponds to the distance from the centre of the halo where the logarithmic slope is the average value between the inner and outer slope, $-(\beta + \gamma)/2$. Note that in what follows, we choose Δ to depend on the values of Ω and Λ at the time of collapse according to

$$\Delta(\Omega, \Lambda) = 178 \begin{cases} \Omega^{0.30}, & \text{if } \Lambda = 0 ; \\ \Omega^{0.45}, & \text{if } \Omega + \Lambda = 1 ; \end{cases} \quad (2.4)$$

(Lacey & Cole 1993; Eke, Cole & Frenk 1996).

The characteristic density and the concentration are not independent parameters. They are related by the requirement that the mean density inside the virial radius is Δ times the present critical one,

$$\delta_{\text{char}} = \frac{\Delta}{3} \frac{c^3}{I(c)} , \quad (2.5)$$

where

$$I(c) = \int_0^c \frac{x^{2-\gamma} dx}{(1 + x^\alpha)^{(\beta-\gamma)/\alpha}} . \quad (2.6)$$

Finally, the virial mass of the halo M_{vir} is defined as the mass within the virial radius,

$$M_{\text{vir}} = \frac{4}{3} \pi r_{\text{vir}}^3 \Delta \rho_c^0 . \quad (2.7)$$

The general form of equation (2.1) allows one to represent a wide class of popular density profiles by making specific choices only for the exponents α, β, γ , and the product $\rho_c^0 \delta_{\text{char}}$. For example, Gunn & Gott (1972) concluded that gravitational collapse could lead to the formation of virialized haloes with almost isothermal density profiles. This non-singular isothermal sphere corresponds to $(\alpha, \beta, \gamma) \approx (2, 2, 0)$. NFW performed a series of cosmological simulations and found that the density profiles of haloes across a wide range of mass scales could all be fit with $(\alpha, \beta, \gamma) = (1, 3, 1)$. Higher resolution simulations give steeper inner cusps (M99; Ghigna et al. 2000; Jing & Suto 2000; Klypin et al. 2001) with density profiles that have a central cusp $r^{-1.5}$. We shall refer to this steeper density profile as the Moore profile which corresponds to $(\alpha, \beta, \gamma) = (1.5, 3, 1.5)$.

The density profile of equation (2.1) includes as a special case the so-called γ -models (Dehnen 1993; Tremaine et al. 1994),

$$\rho(r) = \frac{(3 - \gamma)M}{4\pi} \frac{a}{r^\gamma (r + a)^{4-\gamma}}, \quad (2.8)$$

where a is the scale radius of the density profile and M is the total mass. Near the centre the density profile has a logarithmic slope of $r^{-\gamma}$ while the outer slope is equal to r^{-4} . The cases $\gamma = 1$ and $\gamma = 2$ correspond to Hernquist (1990) and Jaffe (1983) models respectively. For $\gamma = 3$ we have the limiting case of a point mass. The γ -models have proved very useful in the study of elliptical galaxies and bulges since it provides a good approximation to the $r^{-1/4}$ law. Although their outer logarithmic slope is steeper than the ones found for isolated DM haloes, the γ -models provide a good fit to substructure haloes. These models can be represented in the general formalism of equation (2.1) if we choose $\rho_c^0 \delta_{\text{char}} = (3 - \gamma)M/4\pi a^3$ and $(\alpha, \beta, \gamma) = (1, 4, \gamma)$.

2.3 Model Truncation

Density profiles that have an outer slope of $\beta > 3$ lead to finite mass models. On the other hand, haloes with density profiles that fall off as r^{-3} or less steeply than that have a cumulative mass distribution that diverges logarithmically. This is due to the fact that these profiles are not valid out to arbitrarily large distances, but simply

provide a fit up to about the virial radius. However, one is typically interested only in the dynamics within r_{vir} and therefore we must be able to provide equilibrium models up to this distance. Instead of truncating the profiles sharply at the virial radius which would affect the model's equilibrium, particularly near the truncation radius, we choose an exponential cut-off for $r > r_{\text{vir}}$ following Springel & White (1999). This sets in at the virial radius and turns off the profile on a scale r_{decay} which is a free parameter and controls the sharpness of the transition,

$$\frac{\rho(r)}{\rho_c^0} = \frac{\delta_{\text{char}}}{c^\gamma(1+c^\alpha)^{(\beta-\gamma)/\alpha}} \left(\frac{r}{r_{\text{vir}}}\right)^\epsilon \exp\left[-\frac{r-r_{\text{vir}}}{r_{\text{decay}}}\right] \quad (r > r_{\text{vir}}). \quad (2.9)$$

In order to allow for a smooth transition at $r = r_{\text{vir}}$, we require the logarithmic slope there to be continuous,

$$\left.\frac{d \ln \rho}{d \ln r}\right|_{r=r_{\text{vir}}} = \frac{-\gamma - \beta c^\alpha}{1 + c^\alpha}. \quad (2.10)$$

With this requirement, the exponent ϵ is expressed as a function of the concentration, the parameter r_{decay} , the virial radius of the model, and the values of the exponents α , β , and γ ,

$$\epsilon = \frac{-\gamma - \beta c^\alpha}{1 + c^\alpha} + \frac{r_{\text{vir}}}{r_{\text{decay}}}. \quad (2.11)$$

Note that depending on the adopted model and the value of r_{decay} , this procedure results in some additional mass beyond the virial radius. For example, for a Milky Way sized halo model ($M_{\text{vir}} \approx 10^{12} h^{-1} M_\odot$) with $c = 12$ and a choice of $r_{\text{decay}} = 0.1 r_{\text{vir}}$, the total halo mass is $\approx 10\%$ larger than M_{vir} .

2.4 Distribution Function Calculation

The first step in the calculation of the DF is to determine the Newtonian gravitational potential $\Phi(r)$ that is associated with the density profile $\rho(r)$. We start from the general expression for the density profile given by equation (2.1) and we calculate numerically the potential on a grid using equation (1.3). The grid always encompasses the model and linear interpolation is performed between the grid points when necessary. Results with regards to the calculation of the DF will be presented for models that fall into two categories: a) isotropic models and b) anisotropic models with increasing anisotropy of the type proposed by Osipkov and Merritt (Osipkov 1979; Merritt 1985a,b; hereafter Osipkov-Merritt models).

2.4.1 Isotropic Models

The simplest stellar systems are spherical systems in which the velocity dispersion in the radial direction is equal to each of the dispersions in the tangential direction. In this case the velocity dispersion tensor is said to be isotropic (e.g., BT). The phase-space DF of these systems depends only on the energy per unit mass, $f = f(E)$ and the integral equation (1.2) becomes,

$$\rho(r) = 4\sqrt{2}\pi \int_{\Phi(r)}^0 f(E) \sqrt{E - \Phi(r)} dE, \quad (2.12)$$

with solution (Eddington 1916)

$$f(E) = -\frac{1}{\sqrt{8}\pi^2} \left[\int_0^E \frac{d^2\rho}{d\Phi^2} \frac{d\Phi}{\sqrt{\Phi - E}} + \frac{1}{\sqrt{-E}} \left(\frac{d\rho}{d\Phi} \right)_{\Phi=0} \right]. \quad (2.13)$$

For the basic category of models that we will consider here, the second term of the right-hand side is equal to zero since $(d\rho/d\Phi)_{\Phi=0} \propto (1/r^{\beta-1})_{r \rightarrow \infty} = 0$. The integral that remains will be evaluated numerically. The integrand diverges at one or both of the limits but this is handled using standard techniques such as those found in Press et al. (1986). Expressing the term $(d^2\rho/d\Phi^2)$ as a function of known quantities and their derivatives we get,

$$\frac{d^2\rho}{d\Phi^2} = \left(\frac{r}{GM(r)} \right)^2 \left[r^2 \left(\frac{d^2\rho}{dr^2} \right) + \left(\frac{d\rho}{dr} \right) \frac{2rM(r) - 4\pi r^4 \rho(r)}{M(r)} \right], \quad (2.14)$$

where $M(r)$ is the mass at distance r from the centre. Here $(d\rho/dr)$ and $(d^2\rho/dr^2)$ are the first and second derivatives of the mass density which are given by,

$$\rho'(r) = \frac{d\rho}{dr} = \rho(r) \left[-\frac{\gamma}{r} - \frac{(\beta - \gamma)}{r_s} \frac{(r/r_s)^{\alpha-1}}{1 + (r/r_s)^\alpha} \right], \quad (2.15)$$

$$\frac{d^2\rho}{dr^2} = \rho(r) \left[\left(\frac{\rho'}{\rho} \right)^2 + \frac{\gamma}{r^2} - \frac{(\beta - \gamma)}{r_s^2} \left(\frac{r}{r_s} \right)^{\alpha-2} \frac{(\alpha - 1) [1 + (r/r_s)^\alpha] - \alpha (r/r_s)^\alpha}{[1 + (r/r_s)^\alpha]^2} \right]. \quad (2.16)$$

Equations (2.15) and (2.16) are model dependent whereas equation (2.14) is a general formula that relates the second derivative of the mass density with respect to the gravitational potential to the properties of the spherical stellar system of interest.

We evaluated the DF at values of energy equally spaced in $\ln E$ and checked the accuracy of the integration scheme in two ways. First, we compared the numerically calculated DF's with the exact analytical expressions for a Hernquist profile and a Jaffe model. The fractional error in the numerical calculation of the DF is of the order of 0.1% over the range of energies that correspond to apocentric distances of radial orbits between $10^{-6}r_s$ and 10^6r_s . Second, using equation (2.12), we compared the mass density that is recovered from the numerically calculated DF with the exact expression. The recovered density agrees very well with the exact expression (fractional error less than 0.1%) over the same range of distances.

2.4.2 Anisotropic Models of the Osipkov-Merritt Type

While the isotropic models with $f = f(E)$ are very useful, there is no reason why the DF of a halo could not depend on L as well as E . In the simplest case, the two components of the tangential velocity dispersion are equal, but differ from the velocity dispersion in the radial direction. Hence, these systems have an anisotropic velocity dispersion tensor. A special class of anisotropic models are the Osipkov-Merritt models. The DF of these models depends on E and L only through the variable Q ,

$$Q \equiv -E - \frac{L^2}{2r_a^2} = -\Phi - \frac{1}{2} \left[v_r^2 + v_t^2 \left(1 + \frac{r^2}{r_a^2} \right) \right], \quad (2.17)$$

with the additional constraint that

$$f(Q) = 0 \quad \text{for } Q \leq 0. \quad (2.18)$$

The constraint in equation (2.18) implies that there are no unbound stars in the system and that there are no bound stars on high angular momentum orbits. In equation (2.17), v_t is the transverse velocity and r_a the anisotropy radius that controls the degree of global anisotropy in the velocity distribution. Decreasing the anisotropy radius r_a increases the fraction of stars on radial orbits, and in the limit $r_a \rightarrow 0$, the velocity distribution consists of only radial orbits. Note that at $r = r_a$, the radial motions already dominate the tangential ones by a factor of ~ 1.5 . In the limit where $r_a \rightarrow \infty$ these models reduce to the isotropic ones and the parameter Q becomes the total energy $-E$. The anisotropy parameter $\beta(r)$ for these models

is given by,

$$\beta(r) = \frac{r^2}{r^2 + r_a^2}. \quad (2.19)$$

These models are therefore isotropic near the centre and radially anisotropic at large distances. This trend is similar to that found within cosmological simulations of DM haloes (Cole & Lacey 1996; Thomas et al. 1998).

In this case the fundamental integral equation (1.2) is inverted in a similar way to Eddington's inversion yielding,

$$f(Q) = -\frac{1}{\sqrt{8\pi^2}} \left[\int_0^{-Q} \frac{d^2\rho_1}{d\Phi^2} \frac{d\Phi}{\sqrt{\Phi + Q}} + \frac{1}{\sqrt{Q}} \left(\frac{d\rho_1}{d\Phi} \right)_{\Phi=0} \right], \quad (2.20)$$

where $\rho_1(r) = \rho(r)(1 + r^2/r_a^2)$. Equations (2.15) and (2.16) have to be modified accordingly to account for the change of the density profile from the isotropic case.

2.5 Generation of Initial Conditions

Once the density structure of the halo is specified, the cumulative mass distribution is obtained and the particle positions are trivially initialized from it. Gravitating systems determine the mean gravitational field internally in a self-consistent way depending on the phase-space DF that fully specifies the velocity structure of each stellar model. Provided that this function is known analytically or can be calculated numerically, the particle velocities are initialized according to the exact velocity distribution. In our models, the particle velocities are sampled from the derived DF's using the acceptance-rejection technique (Press et al. 1986) which works as follows: At the position of each particle we find the local maximum of the DF, f_{\max} . Since the DF's that we will consider here decrease monotonically with the energy, they reach their maximum value when the energy per unit mass, given by $E = \Phi(r) + \frac{1}{2}v^2$, is minimum. Given that the potential is fixed for a given point, the condition of the local maximum of the DF is met when $(v_x, v_y, v_z = (0, 0, 0))$. The next step is to calculate the escape speed, V_{esc} , at the position of the particle and to sample at random three velocity components v_x, v_y, v_z within a sphere with radius V_{esc} . Having the sampled speed of the particle and the potential we can calculate the value of the DF at the sampled point, f_{sampled} . The final step is to choose a random value for the DF, f_{random} , between 0 and f_{\max} . If the value of

the distribution function at the sampled point f_{sampled} is larger than f_{random} , then the velocity is accepted and assigned to the particle. Otherwise, the velocity is rejected and another trial is made. This technique is very efficient in cases where the distribution being sampled is uniform. If the distribution is not very uniform many of the sampled points will be rejected resulting in the method being inefficient. In this case a simple solution is to transform the original variables to coordinates whose distribution is as uniform as possible.

Chapter 3

N-body Realizations of Halo Models

3.1 Preliminaries

A number of N -body realizations were evolved in isolation with the intention to highlight the shortcomings of the local Maxwellian approximation and to check the stability of the initialization procedure described in Chapter 2. In total we set up 5 simulations:

1. An isotropic halo of 3×10^6 particles following the Hernquist density profile with a scale radius equal to $r_s = 10\text{kpc}$. The velocity distribution at each point in space is approximated by a Gaussian with a dispersion given by the solution of the Jeans equation (model A). The total mass of this model is equal to one.
2. A halo of 10^5 particles with an isotropic velocity distribution following the Hernquist density profile and using the initialization procedure described in Section 2 to set up the IC's (model B). The total mass and the scale radius of this model are equal to one.
3. An identical halo to (2) but with an Osipkov-Merritt velocity anisotropy and an anisotropy radius $r_a = 4/3$ (model C).
4. An isotropic halo of 10^6 particles with an NFW density profile and using the initialization procedure described in Section 2 (model D). This model represents a dwarf galaxy with a virial mass of $M_{\text{vir}} = 10^{10} h^{-1} M_{\odot}$ and a concentration of $c = 15$.

5. An identical halo to (4) but following the Moore density profile and having a concentration of $c = 9.5$ (model E).

The simulations were performed with PKDGRAV, a state-of-the-art, multi-stepping, parallel N -body code written by J. Stadel & T. Quinn (see Stadel 2001 for details). The code uses a spline softening length such that the force is completely Newtonian at twice the quoted softening lengths with the equivalent Plummer softening being 0.67 times the spline softening one. We used an adaptive, kick-drift-kick (KDK) leapfrog integrator (Stadel 2001) (requiring that a change in velocity be applied before and after the particle is allowed to "drift" through space) and the individual particle timesteps Δ_t are chosen according to $\Delta_t \leq \eta \sqrt{\epsilon_i / \alpha_i}$, where ϵ_i is the gravitational softening length of each particle, α_i is the value of the local acceleration, and η is a parameter that specifies the size of the individual timesteps and consequently the time accuracy of the integration. In addition, the particle time steps are quantized in power-of-two hierarchy of the largest time step. Note that the time integration was performed with high enough accuracy to ensure that the total energy was conserved to better than 0.3 % in all runs.

For all the models, we follow the time evolution of the density profile $\rho(r)$, the radial velocity dispersion σ_r , the tangential velocity dispersion σ_t , and the velocity anisotropy parameter β . All these quantities are measured directly from the particle distribution by binning particles in spherical shells and the errors in the density plots are standard Poisson errors associated with the number of particles in each bin. All quantities are plotted from the softening length, $r = \epsilon$. We have also explicitly checked that none of our results are compromised by choices of force softening, time-stepping or opening angle criteria in the treecode.

3.2 Models Generated Under the Local Maxwellian Approximation

Figure 3.1 presents results for the halo model A. This model has been generated assuming that the velocity distribution at any given point is a Gaussian and constructed with a reasonably large scale radius such that the central region having

a slope of r^{-1} is adequately probed. We plot the density profile and the velocity structure for four different times (initially and after 0.3, 1 and 2 crossing times at the scale radius). A number of points can be made from the results shown in these plots. First, we observe that the central density cusp evolves quite rapidly into a constant density core (only after 0.3 crossing times at the scale radius). The central density cusp then starts to fluctuate and relaxes after some time having a logarithmic slope much shallower than the initial r^{-1} . Second, the change in the velocity structure is notable. The radial and tangential velocity dispersions evolve significantly over the timescales of these runs. The initial values of σ_r and σ_t change by $\sim 10\%$ and the evolution of the anisotropy parameter β shows that the initially isotropic model evolves into a radially anisotropic one. Note that two-body relaxation or \sqrt{N} mass fluctuations are not responsible for the observed evolution since the time-scale is too short – the instability develops on a single core crossing time. Instabilities that arise from the Local Maxwellian approximation and propagate outwards are the cause of the observed evolution.

In order to further investigate the effect of the approximate scheme on the velocity structure of the evolved N -body haloes, we generated two Hernquist models having 10^5 particles. The first model has an isotropic velocity dispersion tensor and the second one has an Osipkov-Merritt velocity anisotropy with an anisotropy radius equal to $r_a = 4/3$. Results are presented in a system of units where the gravitational constant, G , the scale radius of the halo, r_s and the halo mass within the scale radius, $m(r_s)$ are all equal to unity. With this choice of units, the crossing time at the scale radius is $t_{\text{cross}} = \sqrt{r_s^3/Gm(r_s)} = 1$, and we will adopt it as our time unit. The half-mass radius of the models is $r_h = (\sqrt{2} + 1)r_s \simeq 2.41$ and the orbital time-scale at the half-mass radius is $t_h = 2\pi r_h/Vc(r_h) \simeq 16.6$ time units. We ran these models to $t = 100$ or approximately 6 orbital times at the half-mass radius and we plot the evolution of the radial velocity dispersion and the anisotropy parameter β in Figure 3.2. The two upper panels in Figure 3.2 present results for the initially isotropic model, while the two lower panels show the evolution of the anisotropic one. Note that the simulation time-scales are much longer than those used for model A in order to probe the evolution over the entire systems. Figure 3.2 shows that the velocity structure changes significantly over the entire range of both

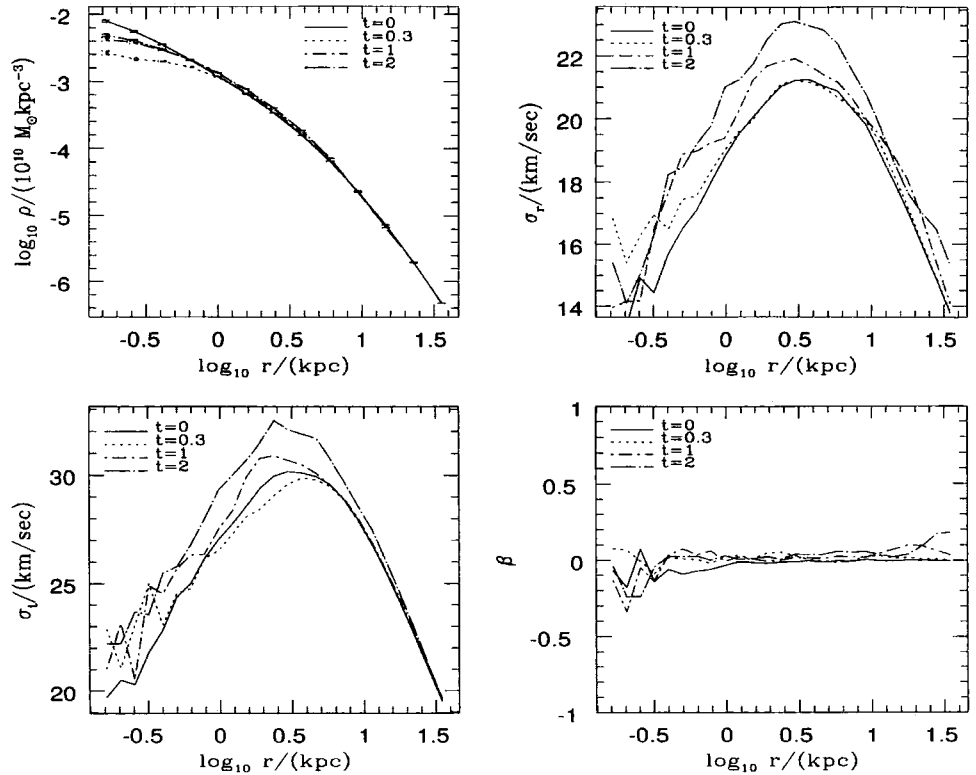


Figure 3.1: Density profile (top left) and velocity structure (radial dispersion (top right), tangential dispersion (bottom left) and anisotropy parameter (bottom right)) as a function of time for model A. The IC's were generated under the local Maxwellian approximation. The solid lines show the initial profiles. The dotted lines show the profiles after 0.3 crossing times at the scale radius. The dashed lines show the profiles after 1 (dot-short) and 2 (dot - long) crossing times at the scale radius. The ratio of the crossing time at the scale radius to that at the half-mass radius is 0.37.

models. These results demonstrate that approximating the DF with only the second moment of the CBE results into a significant evolution of the entire system in the velocity space.

3.3 Velocity Profiles

How do the proper self-consistent velocity profiles differ from a Maxwellian velocity distribution? Figures 3.3, 3.4 and 3.5 present the exact one dimensional velocity distribution sampled from the numerically calculated DF and the Gaussian velocity

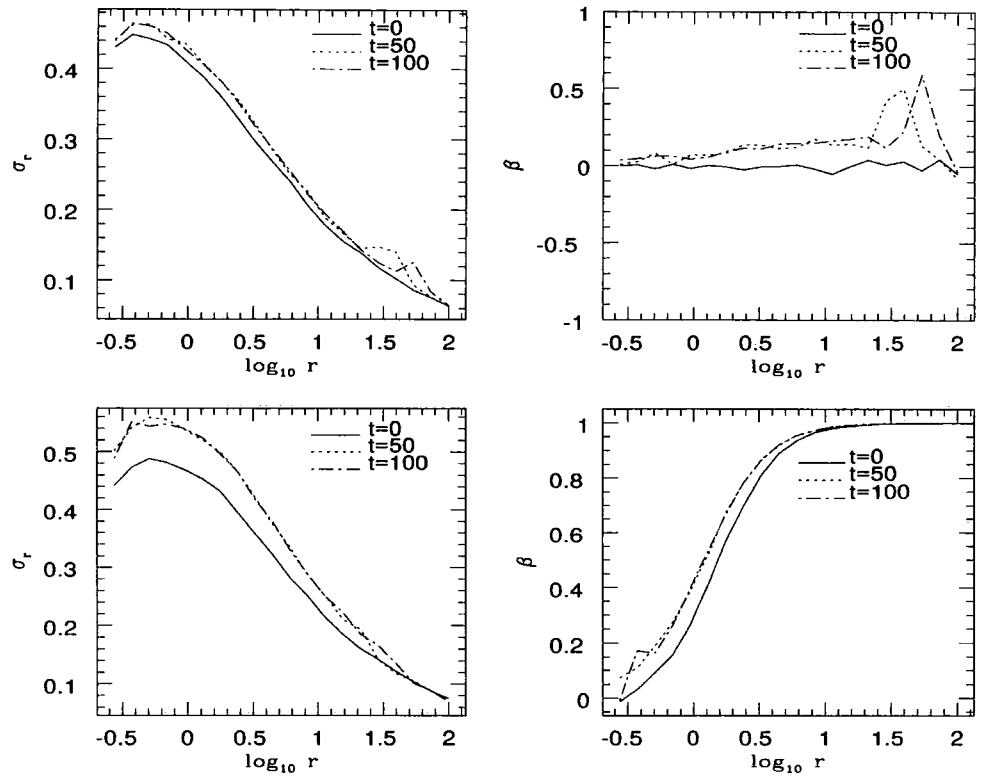


Figure 3.2: Radial velocity dispersion and anisotropy parameter as a function of time for a Hernquist halo having an isotropic velocity dispersion tensor (upper panels) and velocity anisotropy of the Osipkov-Merritt type (lower panels). The solid lines show the initial profiles. The dotted lines show the profiles after 50 crossing times at the scale radius. The dot-short dashed lines show the profiles after 100 crossing times at the scale radius. Both models are simulated with 10^5 particles. See text for the model parameters.

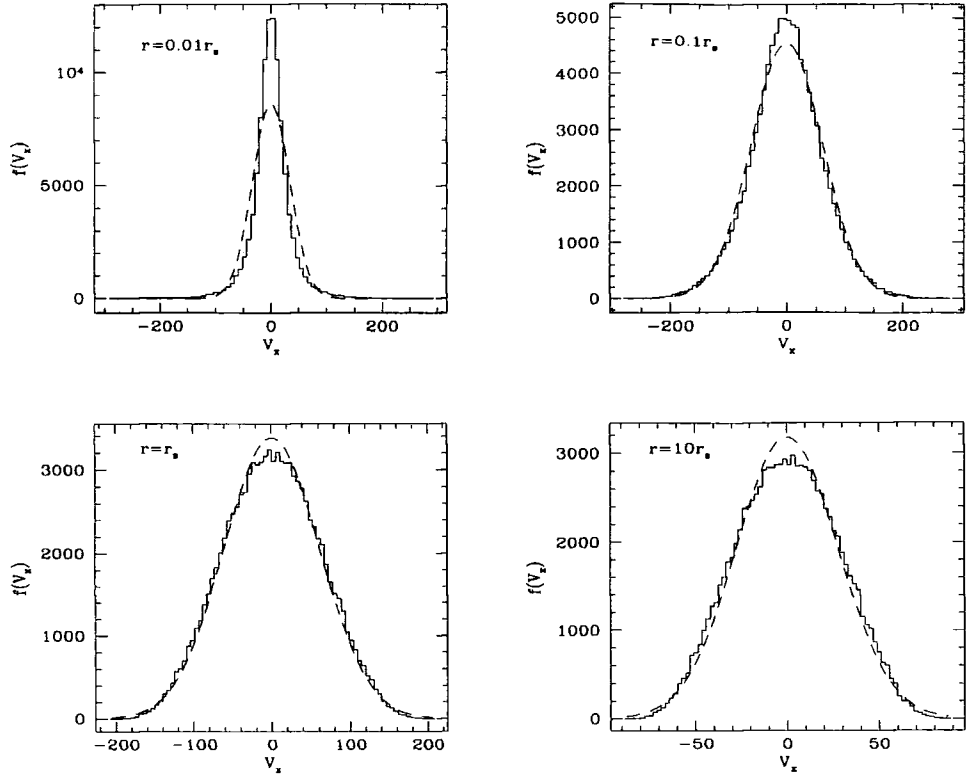


Figure 3.3: Histogram of the one dimensional velocity distributions for an isotropic Hernquist profile for four different distances from the centre. The dashed-lines show the Gaussian velocity distributions with the same second moment.

distribution with the same second moment. Results are presented for three models (Hernquist, NFW and Moore profile) and for four different distances from the model's centre.

A number of remarks can be made from these plots. First, for all three models, the true velocity distribution is more peaked than the Gaussian one near the centre demonstrating that using the local Maxwellian approximation is incorrect. As one moves further out from the centre of the system, the differences between the velocity distributions become smaller, but are still evident. At distances close to the scale radius, the two distributions become closer and the true velocity distribution starts to resemble a Gaussian. Beyond the scale radius the trend is that the true velocity distribution is less peaked than a Gaussian. Second, there are dissimilarities in the behaviour of the models depending on the value of the inner logarithmic slope of the density profile. Specifically, for density profiles with an inner cusp of r^{-1} (e.g., Hernquist, NFW) the differences between the velocity distributions are larger

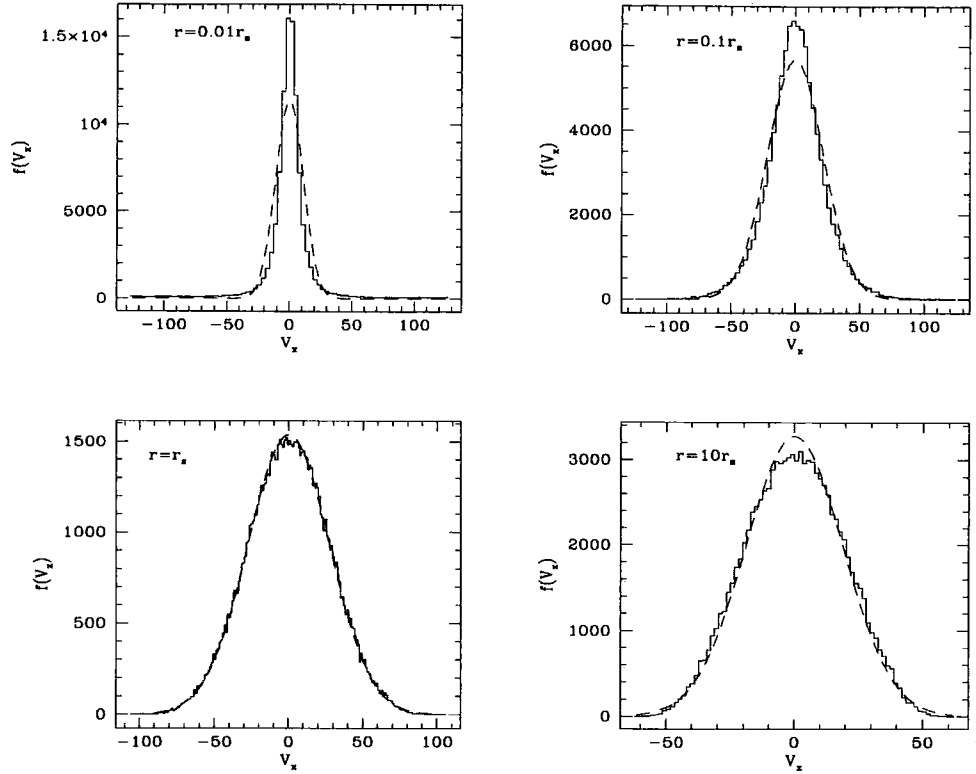


Figure 3.4: Histogram of the one dimensional velocity distributions for an isotropic NFW profile. The line styles and pannels are the same as in Figure 3.3.

near the centre than in cases of density profiles with a steeper inner cusp like the Moore profile. The reason is that as the density slope approaches the value of r^{-2} the profile resembles that of an isothermal sphere for which the distribution of velocities at each point is a Maxwellian.

Finally, Figure 3.6 verifies some of the aforementioned conclusions. In this Figure, we plot the ratios of the true velocity distributions and the Gaussians for the NFW and the Moore density profiles and for the same four distances. The results shown in Figure 3.6 indicate that as we are approaching the model's centre the differences between the distributions become larger and that for the Moore density profile the local Maxwellian approximation works better.

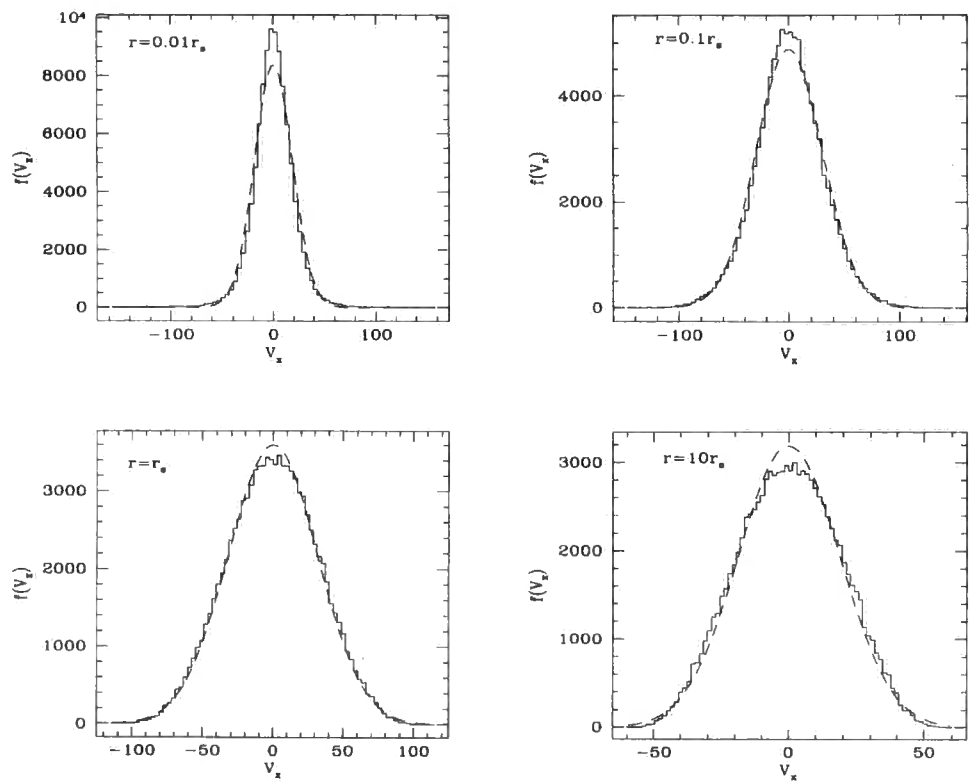


Figure 3.5: Histogram of the one dimensional velocity distributions for an isotropic Moore profile. The line styles and panels are the same as in Figures 3.3 and 3.4.

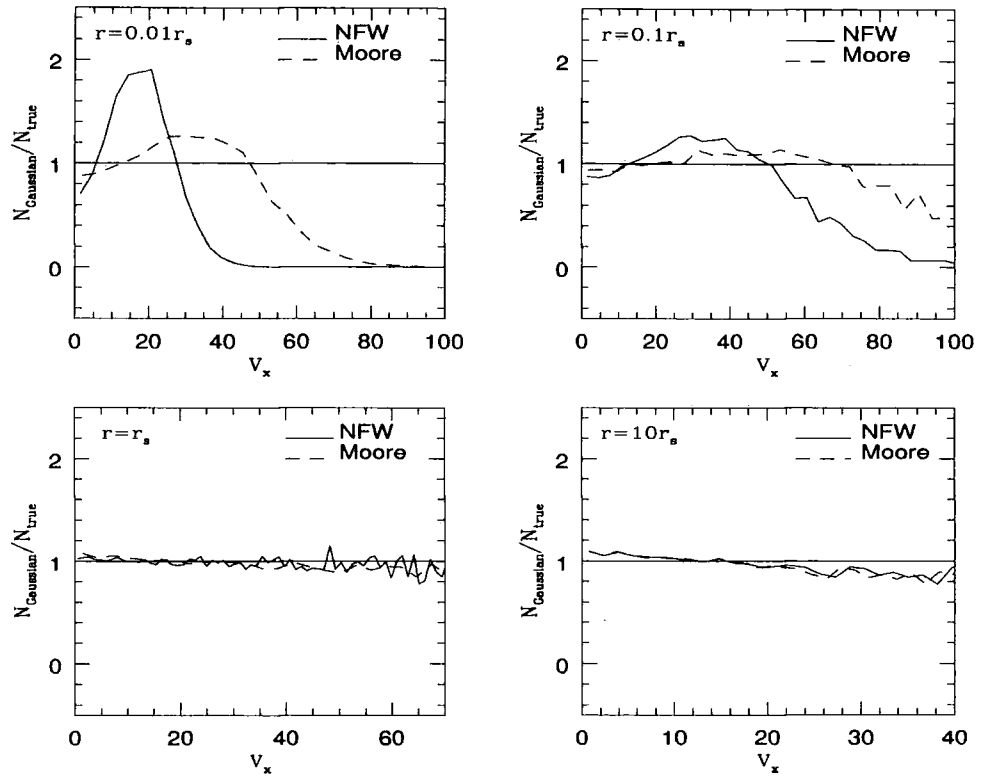


Figure 3.6: Ratios between the true velocity distributions and the Gaussians for four different distances from the model's centre. The solid lines refer to the NFW density profile. The dotted lines refer to the Moore profile. Both models have an isotropic velocity dispersion tensor.

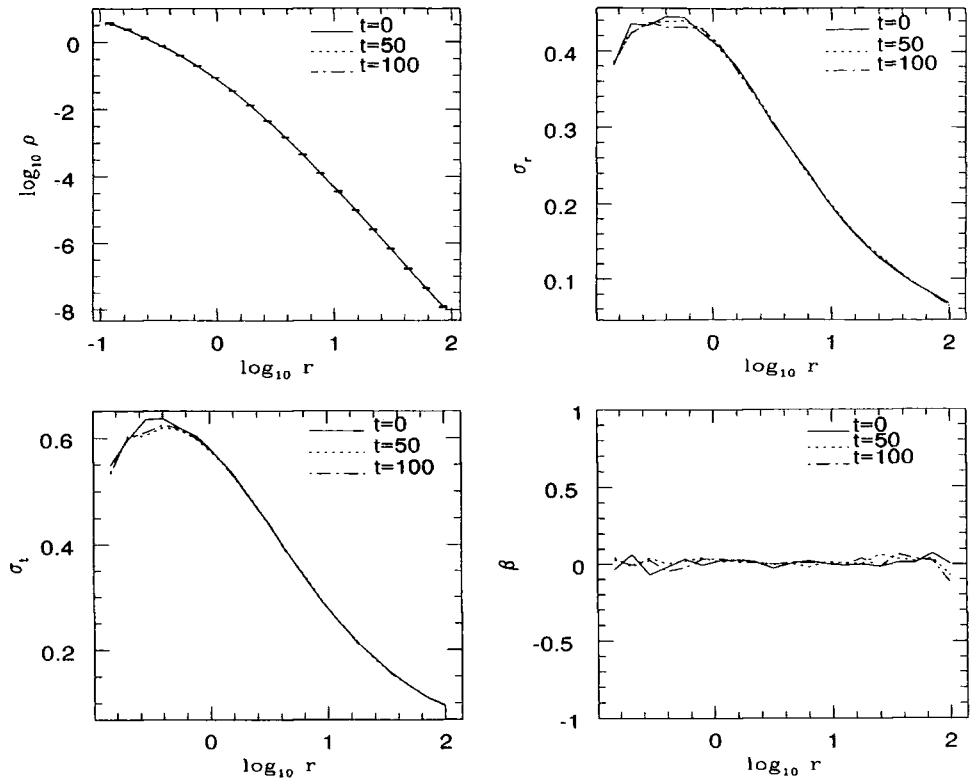


Figure 3.7: Density profile (top left) and velocity structure (radial dispersion (top right), tangential dispersion (bottom left) and anisotropy parameter (bottom right)) as a function of time for an isotropic Hernquist halo (model B). The IC's were generated according to the procedure described in Chapter 2. The line styles and pannels are the same as in Figure 3.2.

3.4 Stability Tests Using the Exact Distribution Function

In Figures 3.7 and 3.8 we show the density profiles and the velocity structure at three times (at times $t=0, 50$ and 100 crossing times at the scale radius) for models B and C respectively. These models were produced according to the procedure outlined in Chapter 2. The timescales are more than sufficient to quantify any deviation from equilibrium. There is essentially no change in the density profiles and the velocity structure over the timescales of our runs. Some minor deviations in the velocity structure at small radii are not the result of the model not being in equilibrium, but are due to Poisson statistics associated with the number of particles in each bin.

The final two simulations were run with the intention of showing the robustness

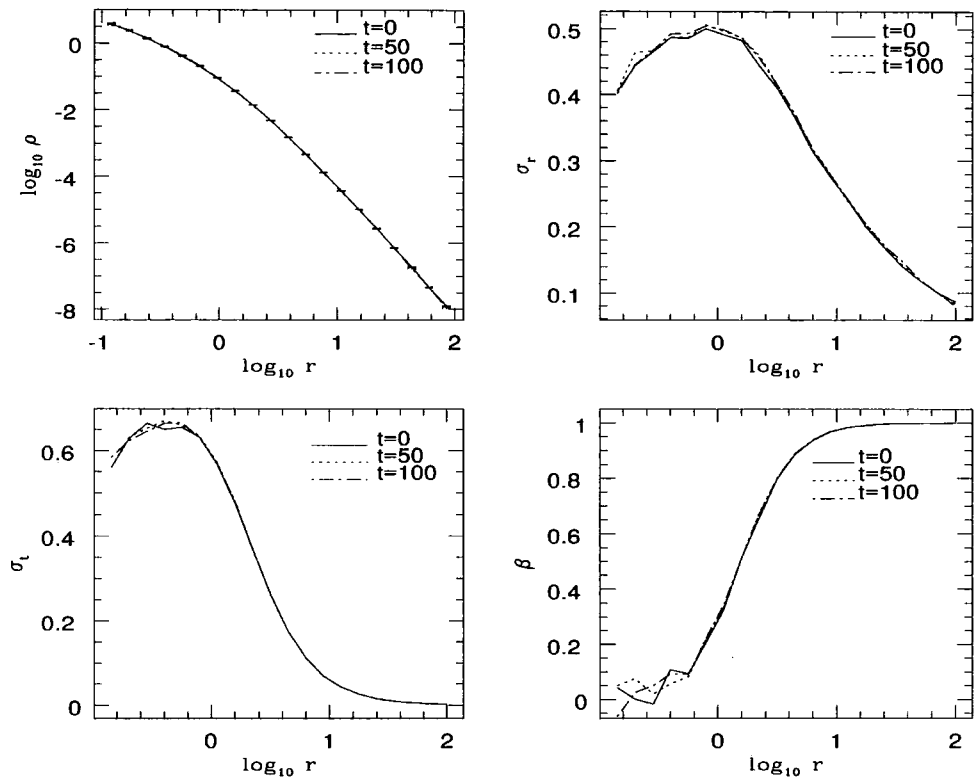


Figure 3.8: Profiles as a function of time for a Hernquist halo with velocity anisotropy of the Osipkov-Merritt type (model C). The particle velocities were sampled from the DF and the panels and line styles are the same as in Figure 3.7.

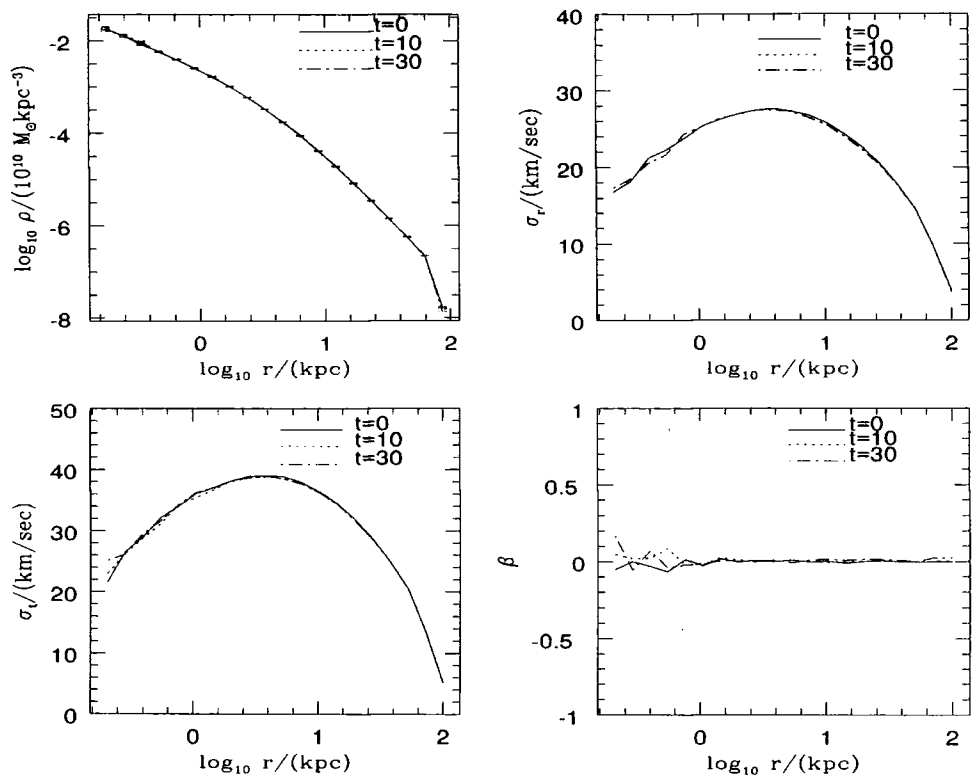


Figure 3.9: Density profile and velocity structure as a function of time for a dwarf galaxy following the NFW density profile(model D). See text for the model parameters. The ratio of the crossing time at the scale radius to that at the virial radius is 5.3^{-3} .

of our adopted procedure. We ran two simulations of a dwarf galaxy having a virial mass of $M_{\text{vir}} = 10^{10} h^{-1} M_{\odot}$. In the first simulation denoted by D the galaxy followed the NFW density profile and had a concentration of $c = 15$. In the second simulation, E, the galaxy followed the Moore density profile and had a concentration of $c = 9.5$. The crossing time at the scale radius for both models is approximately $t_{\text{cross}} \sim 0.1$ Gyrs and the orbital time-scale at the half-mass radius is $t_{\text{h}} \sim 3.3$ Gyrs for the NFW profile and $t_{\text{h}} \sim 3$ Gyrs for the Moore profile. The scale radius of model D is $r_{\text{s}} = 2.94 h^{-1} \text{kpc}$ and we choose a gravitational softening of $\epsilon = 0.105 h^{-1} \text{kpc}$. For model E the scale radius and the chosen softening are $r_{\text{s}} = 4.62 h^{-1} \text{kpc}$ and $\epsilon = 0.196 h^{-1} \text{kpc}$. Finally, we ran our models to $t = 30$ or approximately 1 orbital time at the half-mass radius. The results of these runs are presented in Figures 3.9 and 3.10 and they are quite encouraging. Virtually no evolution can be discerned over the timescales of the runs in the density profile or in the velocity structure of the models.

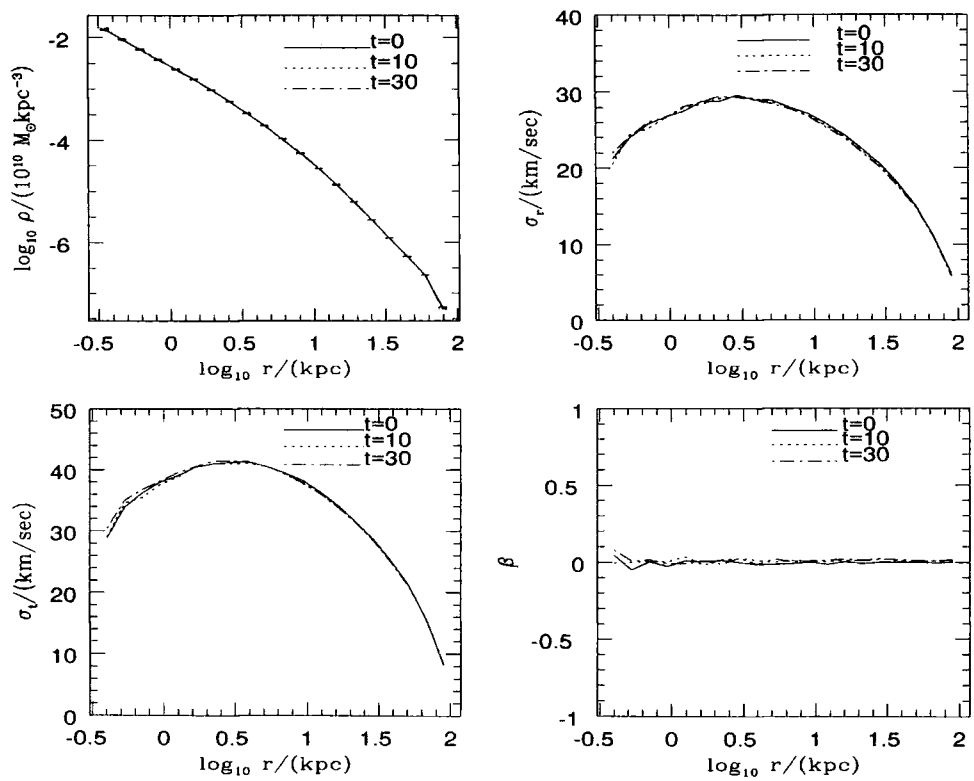


Figure 3.10: Density profile and velocity structure as a function of time for a dwarf galaxy following the Moore density profile(model E). See text for the model parameters. The ratio of the crossing time at the scale radius to that at the virial radius is 0.074.

Chapter 4

Applications

In this chapter four possible applications of our method of constructing equilibrium DM haloes are discussed.

4.1 Collisions of DM Haloes

The study of interactions (mergers and weak collisions) between spherically symmetric systems is vital for the understanding of basic physical processes. During strong encounters between galaxies, each galaxy induces tidal effects in the other, causing significant changes in their structure. As an example, consider the de Vaucouleurs $r^{1/4}$ law that has been extensively used to fit the observed surface brightness profiles of elliptical galaxies and bulges of spiral galaxies. In a study, Makino et al. (1990) showed that strong external disturbances to the gravitational potential of a galaxy produce a remnant that is in good agreement with the de Vaucouleurs law. These kind of perturbations are common in galaxy-galaxy mergers.

On the other hand, the effects of weak collisions in which the systems do not merge, are much less drastic, but potentially more important due to the higher frequency of occurrences. A prominent example are galaxy clusters. Direct major mergers are relatively rare and the bulk of morphological transformation is due to the multiple high-speed encounters between galaxies, a process termed "galaxy harassment" by Moore et al. (1996b). Funato & Makino (1999) performed a series of numerical simulations of passing encounters between identical galaxies. Their results suggest that when galaxies evolve primarily by passing encounters, a relation between the mass and the velocity dispersion develops. Under the assumption of a constant M/L this relation is equivalent to the Faber-Jackson relation which is observed for cluster elliptical galaxies.

The DF's presented in this work provide a motivated set of models for conduct-

ing studies regarding the change of the structural parameters of individual haloes resulting from mergers and passing encounters. Systematic changes in the mass, the energy distribution, and the density profile between the initial models and the remnants can be investigated and quantitative analysis depending on halo models and collision parameters can be done. The density profiles that are included in this study contain many popular forms found in the literature accommodating a wide class of models.

4.2 Relaxation and Evolution of Substructure in Cuspy DM Haloes

The Cold Dark Matter (CDM) paradigm for structure formation (Peebles 1982; Davis et al. 1985) is the most successful and well-motivated cosmological model despite the problems on small scales. One of its most basic premises is that structure forms hierarchically according to the "bottom-up" scenario. Small dense haloes collapse at large redshifts and subsequently merge to form the large virialized systems that contain the galaxies we see today. The complexity of this picture, with continuous mergers, tidal stripping, and potential changes, makes the study of the mechanisms responsible for the evolution of these subhaloes a very difficult issue in a cosmological context. Additionally, the first virialized objects which end up in the central regions of the large haloes, contributing to its central density cusp, contain only very few particles, independent of resolution making them susceptible to numerical artifacts and two-body relaxation. Since usually one is interested in getting the correct dynamics of the haloes near the centre where the galaxy resides, we have to be very careful monitoring these first generation systems.

The models presented here enable one to conduct highly-controlled numerical experiments in order to gain a better understanding of the physical processes at work for which the resolution of cosmological simulation is insufficient. These DF's provide a set of models for the study of the two-body relaxation timescale as a function of the particle number and for the investigation of how the internal structure and kinematics of subhaloes might evolve as they orbit within their host halo.

4.3 Stability Studies

For all spherical stellar systems with an isotropic velocity distribution ($f = f(E)$) there is a criterion sufficient to guarantee stability against both radial and non-radial perturbations. The DF has to be a decreasing function of energy: $df/dE < 0$ (Antonov 1962; Dorémus, Feix, & Baumann 1971). However, the situation for systems with anisotropic velocity distributions ($f = f(E, L)$) is much less clear. Numerical experiments show that systems with predominantly radial orbits ($r_a \rightarrow 0$) are susceptible to form a bar (radial-orbit instability) (Hénon 1973; Palmer & Papaloizou 1987) and numerical linear stability analyses (Saha 1991; Weinberg 1991) have shown that even a small velocity anisotropy can be sufficient to drive a system towards instability. Carollo, de Zeeuw, & van der Marel (1995) studied models having a density power-law fall-off at large distances $\rho \propto r^{-4}$ and found that the stability boundary depends on the shape of the potential and that the DF becomes negative for values of the anisotropy radius smaller than a threshold value. In addition, Widrow (2000) considered density profiles that fall off as r^{-3} and presented DF's for different values of r_a highlighting the pathological nature of some of them. Furthermore, he concluded that the issue of instability is more severe in these models since the threshold value of r_a above which physical models exist is larger. The DF's calculated in this study may provide a tool to further investigate these issues and determine stability boundaries and regions where physical models exist.

4.4 Multicomponent Models

The single component models that we presented here are suitable for the modeling of spherical DM haloes and stellar distributions. Nevertheless, the task of setting up a self-consistent disc galaxy models has proved to be a daunting one. Recent strategies to handle this problem have included solving the only non-trivial Jeans equation for each component separately and realizing the particle velocities with Gaussians (Hernquist 1993), or choosing for each component analytical forms for the DF in terms of known integrals of motion, calculating the combined potential

and using it for the velocity sampling (Kuijken & Dubinski 1995). Relaxation from non-equilibrium IC's and density profiles that do not fit in a complete cosmological setting are among the drawbacks of these approaches. Unfortunately, the extension of our technique to encompass disk models is not obvious, since for multi-component models one has to solve the Poisson's equation for the total potential and to numerically invert equation (1.2) in the presence of the disk. This procedure is cumbersome since the DM halo will not remain spherically symmetric. However, our models can be used as a starting point to numerically construct self-consistent two component models, consisting of either a stellar distribution and a black hole or a stellar distribution embedded in a DM halo (stellar component + DM). Analytical studies in this field have been carried out by numerous authors. For example, Tremaine et al. (1994) generalized the γ -models to a two-parameter family, in which the galaxy contains a black hole and can be useful for illustrating the behaviour of the central parts of galaxies. Moreover, Ciotti (1996) presented the analytical DF for a system consisting of a stellar distribution and a DM halo, both following the Hernquist density profile, but with different total masses and scale radii. It would be very interesting to investigate this special class of multi-component models and possibly to include other types of velocity anisotropy (e.g., constant anisotropy throughout the model and/or modifications of the Osipkov-Merritt type with constant anisotropy near the centre). In addition, there is evidence that the Osipkov-Merritt models are extremely prone to the $l=2$ (radial orbit) instability since at large radii they become completely radial. A superposition of the latter models with the isotropic ones would not have this feature. The conduction of all these studies is planned for the near future since they fall beyond the scope of this thesis.

Chapter 5

Conclusions

Building isolated haloes for conducting numerical experiments is a popular and useful approach for studying the behaviour of systems in the non-linear regime. In the majority of these experiments, very simple density profiles including King models (King 1966), the Plummer model (Plummer 1911), and isothermal spheres were used to set up the IC's of the systems of interest. This choice was imposed mainly for simplicity (e.g., existence of simple potential-density pairs and analytic DF's) and lacks the accuracy of an approach stemming from pure cosmological considerations. In this study, we have concentrated on the problem of solving the coupled equations (1.1) and (1.3) with the intention of constructing self-consistent models of DM haloes following any desired density profile. The adopted procedure has two steps. The first step involves the calculation of the gravitational potential through Poisson's equation, with the second step being the numerical inversion of the fundamental integral equation (1.2). We have evolved a number of particle distributions that have different density profiles and velocity dispersion tensors. These distributions were constructed with two separate methods: a) the exact method in which the velocities are sampled from the model's DF and b) the approximate scheme of assuming that the velocity distribution at each point is a Gaussian. Our motives have been to investigate the stability of the models generated using these different techniques. As expected, models constructed using the procedure outlined in Chapter 2 are very stable whilst the approximate technique has a number of shortcomings that lead to strong evolution in the central density profile and orbital anisotropy over the entire model.

The mass density profiles that exist in the literature can be divided into two general families. The first family consists of simple potential-density pairs that are extremely useful for the dynamical modelling and the understanding of various physical processes that take place in galaxies. These models are ideal as simple

galaxy models and their importance lies in the fact that many of their properties, including the DF, are known analytically. Simple analytical models such as the Plummer model, the King profile, and the γ -models with special cases including the Hernquist (Hernquist 1990) and the Jaffe profile (Jaffe 1983), belong to this family. These models (mostly generated with an isotropic velocity distribution) have many uses including the modelling of elliptical galaxies and of bulges of spiral galaxies, and they can provide insight into the behaviour of real systems. The second family is related to recent high resolution cosmological N -body simulations. These simulations favour DM density profiles that do not share the analytical simplicity of those belonging to the first family (e.g., the NFW, the Moore density profile). These profiles have been studied extensively and have received a lot of theoretical attention. For example, there is a longstanding debate over the value of the central density slope, whereas it seems that a consensus exists with regards to their power-law falloff at large distances. The DF's for these popular DM density profiles can only be derived numerically, thus limiting the simplicity of creating N -body realizations of halo models that originate from pure cosmological considerations. Moreover, in the great majority of the numerical experiments so far, the velocity dispersion tensor has been assumed isotropic, inconsistently with what one expects for a realistic halo model. For example, the radial orbits that we primarily expect in the outer regions of the halo are consistent with the Osipkov-Merritt type for the velocity dispersion tensor.

Our algorithm deals with both families of density profiles and its main purpose is to numerically generate IC's for N -body experiments that are under the full control of the experimenter. Moreover, our algorithm accommodates two types of dispersion tensors: (a) isotropic and (b) anisotropic of the type proposed by Osipkov and Merritt. Thus, the structure and velocity distributions of our DM halo models are consistent with the predictions of the hierarchical structure formation models. As expected, models constructed using the procedure outlined in Chapter 2 are very stable whilst the approximate technique has a number of shortcomings that lead to strong evolution in the central density profile and orbital anisotropy over the entire model.

Appendix 1

Computer Programs Available

The computer programs that we have designed in the course of this study are written in standard FORTRAN 90 and contain the following features:

1. A code to calculate all the important dynamical properties (e.g., the mass $M(r)$, the gravitational potential $\Phi(r)$) of a spherical stellar system for a given density profile. Moreover, the code calculates the radial velocity dispersion σ_r by solving the only non-trivial Jeans equation for any given value of the anisotropy parameter β . Everything is calculated on a grid and linear interpolation is applied between the grid points. This code can easily be extended to accommodate properties such as the kinetic energy $T(r)$, the potential energy $W(r)$, and projected quantities such as the projected mass density $\Sigma(R)$ and the line-of-sight velocity dispersion $\sigma_{los}(R)$.

2. A code that inverts equation (1.2) and calculates the DF for any given density profile and for the two categories of velocity dispersion tensors that we considered here (isotropic models and models of the Osipkov-Merritt type velocity anisotropy).

3. A code to generate the IC's by sampling the phase-space points from the density profile and the DF according to the method described in Chapter 2.

These programs are electronically available from the authors upon request. We anticipate to include additional anisotropic models in the next version of the code which will become publicly available. Moreover, we hope to implement in the future, our stable cosmologically motivated DM halo models to set up a completely stable three-dimensional self-consistent disk for N -body experiments.

Appendix 2

The Moore Density Profile

In this Appendix, we find analytical solutions for the mass distribution, the gravitational potential, the orbital frequency, the circular speed and the radial velocity dispersion of the Moore density profile. We describe the dependence of these parameters on the concentration of the halo and we express them in terms of an observable quantity: the maximum circular speed V_{max} . The Moore density profile has the form,

$$\frac{\rho(r)}{\rho_c^0} = \frac{\delta_{char}}{(r/a)^{1.5} [1 + (r/a)^{1.5}]} . \quad (7.1)$$

The characteristic density δ_{char} is given by,

$$\delta_{char} = \frac{\Delta c^3 g(c)}{3} , \quad (7.2)$$

where

$$g(c) = \frac{1}{(2/3) \ln(1 + c^{1.5})} . \quad (7.3)$$

It is possible to quantify a relation between the concentration parameters of the NFW and Moore profiles. In the case of the NFW profile the maximum of the circular speed (corresponds to a region where the logarithmic slope of the density profile is equal to the isothermal value of $d \ln \rho / d \ln r = -2$) occurs at a distance equal to r_s . In the Moore profile, this distance is approximately $0.63a$. If we want now to scale both profiles to match at the maximum of the circular speed, we have to put $r_s \approx 0.63a$. This relation can be extended into a relation between the concentrations of the two profiles since for a given mass the virial radii are the same. Thus, $c_{moore} \approx 0.63 c_{nfw}$. Typical values for the concentration range from $c_{moore} \approx 10$ for dwarf galaxy size halos ($M_{vir} \approx 10^9 h^{-1} M_\odot$) to $c_{moore} \approx 3.5$ for cluster size halos ($M_{vir} \approx 10^{15} h^{-1} M_\odot$).

It is convenient to express the distance from the center of the object in units of the virial radius r_{vir} ,

$$s = \frac{r}{r_{\text{vir}}} . \quad (7.4)$$

The density profile of equation (7.1) then becomes,

$$\frac{\rho(s)}{\rho_c^0} = \frac{\Delta c^{1.5} g(c)}{3s^{1.5}(1 + (cs)^{1.5})} . \quad (7.5)$$

The mass distribution in units of the virial mass follows from equations (7.3) and (7.5),

$$\frac{M(s)}{M_{\text{vir}}} = g(c) \left[\frac{2}{3} \ln(1 + (cs)^{1.5}) \right] . \quad (7.6)$$

From the last equation it is clear that the mass distribution diverges at large distances. This constitutes a drawback of the model from a physical point of view.

The gravitational potential associated with the Moore density profile is given by:

$$\Phi(s) = -\frac{GM_{\text{vir}}}{r_{\text{vir}}} c g(c) \tilde{K}(s) , \quad (7.7)$$

where

$$\tilde{K}(s) = \frac{1}{g(cs) cs} + \frac{\pi}{\sqrt{3}} - \frac{1}{3} \ln \left[\frac{cs + 2\sqrt{cs} + 1}{cs - \sqrt{cs} + 1} \right] - \frac{2}{\sqrt{3}} \arctan \frac{2\sqrt{cs} - 1}{\sqrt{3}} . \quad (7.8)$$

From equations (7.7) and (7.8) we see that the gravitational potential at the center, $\Phi(0) = -(GM_{\text{vir}}/r_s)g(c)(4\pi/3\sqrt{3})$ is finite.

The orbital frequency of circular orbits $\Omega(r)$ is defined by $\Omega^2(r) = GM(r)/r^3$ leading to,

$$\Omega^2(s) = \frac{GM_{\text{vir}} g(c)}{r_{\text{vir}}^3 s^3} \left[\frac{2}{3} \ln(1 + (cs)^{1.5}) \right] . \quad (7.9)$$

The circular speed of a spherical halo defined to be the speed of a test particle in a circular orbit at radius r is given by,

$$V^2 = \frac{GM(r)}{r} . \quad (7.10)$$

Following from equation (7.10) we have

$$V^2(s) = \frac{GM_{\text{vir}} g(c)}{r_{\text{vir}} s} \left[\frac{2}{3} \ln(1 + (cs)^{1.5}) \right] . \quad (7.11)$$

A more robust quantity to define the halo properties is the maximum circular speed V_{max} . This parameter is more easily related to an observable quantity and

therefore is preferable to the halo mass or the halo concentration. For the Moore density profile the maximum circular speed occurs at $r_{\max} \approx 1.25r_s$. All the physical quantities of interest can now be expressed in terms of this speed,

$$V_{\max}^2 = \frac{GM_{\text{vir}}}{1.25r_s} \times \frac{g(c)}{g(1.25)}, \quad g(1.25) \approx 1.7153 \quad (7.12)$$

$$M(s) = \frac{1.25r_s V_{\max}^2}{G} \times \frac{g(1.25)}{g(cs)}, \quad (7.13)$$

$$\Phi(s) = -1.25V_{\max}^2 g(1.25) \tilde{K}(s), \quad (7.14)$$

$$\Omega^2(s) = \frac{1.25V_{\max}^2}{r_s^2 c^3} \times \frac{g(1.25)}{s^3 g(cs)}. \quad (7.15)$$

The radial velocity dispersion $\sigma_r(r)$ can be obtained by solving the Jeans equation. This equation under the assumption of spherical symmetry and no rotation reads,

$$\frac{1}{\rho} \frac{d}{dr} (\rho \sigma_r^2) + 2\beta \frac{\sigma_r^2}{r} = -\frac{d\Phi}{dr}, \quad (7.16)$$

where β the anisotropy parameter. We will present the solutions of the Jeans equation for two important cases:

1. We will consider the case where β is constant. Taking into account the boundary condition $\sigma_r \rightarrow 0$ at $s \rightarrow \infty$ the solution to the Jeans equation reads,

$$\sigma_r^2 = \frac{2}{3} V_{\text{vir}}^2 g(c) [1 + (cs)^{1.5}] s^{1.5-2\beta} \int_s^\infty s^{2\beta-3.5} \left[\frac{\ln(1 + (cs)^{1.5})}{(1 + (cs)^{1.5})} \right] ds. \quad (7.17)$$

2. For the Osipkov-Merritt model the solution to the Jeans equation is,

$$\sigma_r^2 = \frac{2}{3} V_{\text{vir}}^2 g(c) \frac{s^{1.5} [(1 + (cs)^{1.5})]}{s^2 + s_a^2} \int_s^\infty \frac{\ln[1 + (cs)^{1.5}]}{[1 + (cs)^{1.5}]} \frac{(s^2 + s_a^2)}{s^{3.5}} ds. \quad (7.18)$$

Bibliography

- [1] Aguilar, L. A., & White, S. D. M. 1985, *ApJ*, 295, 374
- [2] Antonov, V. A. 1962, *Vestnik Leningradskogo Univ.* 19, 96; English translation in *IAU Symp. 127, Structure and Dynamics of Elliptical Galaxies*, ed. T. de Zeeuw (Dordrecht: Reidel), 531
- [3] Binney, J. & Tremaine, S. 1987, *Galactic Dynamics*. Princeton University Press.
- [4] Boily C. M., Kroupa P., & Peñarrubia-Garrido, J. 2001, *NewA*, 6, 27
- [5] Carollo, C. M., de Zeeuw, P. T., & van der Marel, R. P. 1995, *MNRAS*, 276, 1131
- [6] Ciotti, L. 1996, *ApJ*, 471, 68
- [7] Cole, S., & Lacey, C. 1996, *MNRAS*, 281, 716
- [8] Colpi, M., Mayer, L., & Governato, F. 1999, *ApJ*, 525, 720
- [9] Davis, M., Efstathiou, G., Frenk, C. S., & White, S. D. M. 1985, *ApJ*, 292, 371
- [10] Dehnen, W. 1993, *MNRAS*, 265, 250
- [11] Dorémus, J.P., Feix, M. R. & Baumann G. 1971, *Phys. Rev. Lett.*, 26, 572
- [12] Dubinski, J., & Carlberg, R. 1991, *ApJ*, 378, 496
- [13] Eddington, A. S. 1916, *MNRAS*, 76, 572
- [14] Eke, V. R., Cole, S., & Frenk, C. S. 1996, *MNRAS*, 282, 263
- [15] Font, A. S., Navarro, J. F., Stadel, J., & Quinn, T. 2001, *ApJ*, 563, L1

- [16] Fukushige, T., & Makino, J. 1997, ApJ, 477, L9
- [17] Funato, Y., & Makino, J. 1999, AJ, 511, 625
- [18] Ghigna, S., Moore, B., Governato, F., Lake, G., Quinn, T. & Stadel, J., 2000, ApJ, 544, 616
- [19] Gunn, J.E., & Gott, J.R. 1972, ApJ, 176, 1
- [20] Hayashi et al. 2002, ApJ, submitted (astro-ph/0203004)
- [21] Hénon, M. 1973, A&A, 24, 229
- [22] Hernquist, L. 1990, ApJ, 356, 359
- [23] Hernquist, L. 1993, ApJS, 86, 389
- [24] Jaffe, W. 1983, MNRAS, 202, 995
- [25] Jing, Y.P. & Suto, Y. 2000, ApJ, 529L, 69
- [26] King, I. R. 1966, AJ, 71, 64
- [27] Klypin, A., Kravtsov, A.V., Bullock, J.S. & Primack, J.R. 2001, ApJ, 554, 903
- [28] Kravtsov, A. V., Klypin, A. A., Bullock, J. S., & Primack, J. R. 1998, ApJ, 502, 48
- [29] Kuijken, K., & Dubinski, J. 1994, MNRAS, 269, 13
- [30] Kuijken, K., & Dubinski, J. 1995, MNRAS, 277, 1341
- [31] Lacey, C., & Cole, S. 1993, MNRAS, 262, 627
- [32] Lynden-Bell, D. 1962, MNRAS, 124, 1
- [33] Mayer, L., Moore, B., Quinn, T., Governato, F., & Stadel, J. 2002, MNRAS, 336, 119
- [34] Makino, J., Akiyama, K., & Sugimoto, D. 1990, PASJ, 42, 205
- [35] Merritt, D. 1985a, AJ, 90, 1027

- [36] Merritt, D. 1985b, MNRAS, 214, 25P
- [37] Mihos, J. C., McGaugh, S., & de Blok, W. J. G. 1997, ApJ, 477, L79
- [38] Moore B., Katz N., & Lake G., 1996a, ApJ, 457, 455
- [39] Moore B., Katz N., Lake G., Dressler A., & Oemler A., 1996b, Nature, 379,613
- [40] Moore, B., Governato, F., Quinn, T., Stadel, J. & Lake, G. 1998, ApJ, 499, L5
- [41] Moore, B., Quinn, T., Governato, F., Stadel, J., & Lake, G. 1999, MNRAS, 310, 1147
- [42] Nararro, J. F., Frenk, C. S., & White, S. D. M., 1996, ApJ, 462, 563
- [43] Osipkov, L. P. 1979, Soviet Astron. Lett., 5, 42
- [44] Palmer, P. L., & Papaloizou J. 1987, MNRAS, 224, 1043
- [45] Peebles, P. J. E. 1982, ApJ, 263, L1
- [46] Plummer H. C. 1911, MNRAS, 71, 460
- [47] Press, W. H., Flannery, B. P., Teukolsky, S. A. & Vetterling, W. T. 1986, Numerical Recipes, Cambridge University Press.
- [48] Quinn, P. J., & Goodman, J. 1986, ApJ, 309, 472
- [49] Saha, P. 1991, MNRAS, 248, 494
- [50] Springel, V., & White, S. D. M. 1999, MNRAS, 307, 162
- [51] Stadel, J. 2001, PhD thesis, U.Washington.
- [52] Taylor, J. E., & Babul, A. 2001, ApJ, 559, 716
- [53] Thomas, P., et al. 1998, MNRAS, 296, 1061
- [54] Tremaine, S., et al. 1994, AJ, 107, 634
- [55] van den Bosch, F., Lewis, G., Lake, G., & Stadel, J. 1999, ApJ, 515, 50
- [56] Velázquez, H. & White S. D. M. 1995, MNRAS, 275, 23L

- [57] Velázquez, H., & White, S. D. M. 1999, MNRAS, 304, 254
- [58] Weinberg, M. D. 1991, ApJ, 368, 66
- [59] White, S. D. M., & Rees, M. J. 1978, MNRAS, 183, 341
- [60] Widrow, L.M. 2000, ApJS, 131, 39
- [61] Zhao, H. S. 1996, MNRAS, 278, 488

